Journal of AI and Data Mining
Vol 7, No 4, 2019, 495-506
DOI: 10.22044/JADM.2019.7434.1884

Robust Iris Recognition in Unconstrained Environments

A. Noruzi[1], M. Mahlouji[2,*] and A. Shahidinejad [1]

1. Department of Computer Engineering, Qom Branch, Islamic Azad University, Qom, Iran.
2. Department of Electrical & Computer Engineering, Kashan Branch, Islamic Azad University, Kashan, Iran.

Received 06 September 2018; Revised 22 February 2019; Accepted 08 May 2019
**Corresponding author: mmahlouji@yahoo.com (M. Mahlouji).*

Abstract
A biometric system provides the automatic identification of an individual based on a unique feature or characteristic possessed by him/her. Iris recognition (IR) is known to be the most reliable and accurate biometric identification system. The iris recognition system (IRS) consists of an automatic segmentation mechanism, which is based on the Hough transform (HT). The IRS is divided into six stages including imaging, pre-processing, segmentation, normalization, feature extraction and matching. Through this method, first, a photo is taken from the iris, and then edge detection is done. Later, on a contrast, adjustment is persecuted in the pre-processing stage. Circular HT is subsequently utilized for localizing circular area of the iris inner and outer boundaries. Also, through applying parabolic HT, boundaries are localized between the upper and lower eyelids. The proposed method, in comparison with the available IRSs, not only enjoys a higher accuracy, but also competes with them in terms of the processing time. Experimental results on the images available in the UBIRIS, BATH, CASIA, and MMUI databases show that the proposed method has an accuracy rate of 99.12%, 97, 98%, 98.80%, and 98.34%, respectively.

Keywords: *Hough Transform, Biometric Identification, Segmentation, Normalization, Matching.*

1. Introduction

The human iris contains rich texture, which is highly stable and distinctive. Iris recognition (IR) is a biometric technology that utilizes pattern recognition techniques on the basis of iris high quality images, and has become one of the most promising technologies for biometric authentication. The existing state-of-the-art IR algorithms have achieved remarkable performances, since in comparison with other features utilized in biometric systems, iris patterns are more stable and reliable, and IR is known to be one of the most outstanding biometric technologies [1]. IR for iris images, which are taken distantly from the sensor, is a major challenge of the biometric platform. Additionally, in an unconstrained environment, iris may have occlusions caused by the upper or lower eyelids or eyes may be rolling left or right. In this paper, we try to address such issues. The algorithm has been proposed in [2], where one method stage accurately localizes the iris by a model designed on the basis of the Histograms of Oriented Gradient (HOG) descriptor and Support Vector Machine (SVM), namely HOG-SVM. Based on this localization, iris texture is automatically extracted by means of a cellular automata that evolved through the Grow-Cut technique. Daugman's [3] and Wildes' [4] systems are the two earliest and most famous iris recognition systems (IRSs) containing all IR stages. In the Daugman's algorithm, an iris with two circles that are not necessarily concentric forms the model. Each circle is defined by three parameters (x_0, y_0, r) in a way that (x_0, y_0) determines the center of a circle with the radius of r. An integro-differential operator is used to estimate the values of the three parameters for each circular boundary, and the whole image is searched in relation to the increment of radius r. In Wildes' system, gradient-based Hough transform (HT) has been used to localize two iris circular boundaries. This system consists of two stages. First, a binary map is produced from the image edges by a Gaussian filter. Then an the analysis is performed in a circular Hough space in order to estimate the three

parameters (x_0, y_0, r) for a circle. In [5], iris images are projected vertically and horizontally to estimate the center of the iris. IRS usually consists of three component stages: iris segmentation, feature extraction, and iris matching. Currently, iris segmentation and feature extraction for the captures in less-constrained environments have been extensively investigated in [6]. The algorithm in [7] proposes a computationally efficient iris segmentation approach for segmenting iris images acquired from at-a-distance and under less-constrained imaging conditions. The proposed segmentation approach is developed based on the cellular automata that evolve through using Grow-Cut algorithm. Also an IRS has been proposed in [8], which is used for frontal iris images and for an iris image that is not taken from a frontal view. In this system, when a frontal image is not available for a particular individual, the issue is addressed via maximizing Hamming distance (HD) between the two mentioned images or by minimizing Daugman's integra-differential operator, and then the image is transformed into a frontal image. An algorithm is presented to find eyelash and eyelids occlusions on iris in a completely close-up image similar to Daugman's method in [9]. The algorithm proposed in [10] describes an efficient way for IR by characterizing the key local variations. The basic idea is that local sharp variation points, which denote the appearing or vanishing of an important image structure, should be utilized to represent the characteristics of an iris. The paper [11] proposed a novel texture feature for IR. During pre-processing, iris is segmented using constrained circular HT, which reduces both time-and space-complexity. Through this, a novel texture code matrix is generated, which is then used to obtain a co-occurrence matrix. The algorithm in [12] proposed a reliable iris localization algorithm. It includes localizing a coarse iris location in the eye image using the HT and image statistics; localizing the pupillary boundary using a bi-valued adaptive threshold and the two-dimensional (2D) shape properties; localizing the limbic boundary by reusing the Hough accumulator and image statistics; and regularizing these boundaries using a technique based on the Fourier series and radial gradients. In [13], it is suggested that data reduction has the highest impact on the iris segmentation. Since segmentation is also the first step in the pipeline, this potentially affects the performance of later steps as well, and is therefore of particular importance. Reference [14] introduces a noise-resistant and computational efficient segmentation approach towards less constrained IR. The proposed segmentation approach is based on a modified and fast HT augmented with a newly developed strategy to define iris boundaries with multi-arcs and multi-lines.

The remainder of this paper is organized as follows. In Section 2, the proposed method of IR is introduced, and next, in Section 3, experimental results of the proposed method on several databases are presented, and finally, in Section 4, conclusions are drawn.

2. Proposed method for iris recognition

Figure 1 shows the block diagram for a biometric system of IR in unconstrained environments in which the function of each block is briefly discussed as follows:

1) **Image acquisition**
   At this stage, we capture the iris images using different cameras or from the databases like UBIRIS [15], CASIA [16], MMUI [17], and BATH [18].

2) **Pre-processing**
   Involving edge detection, contrast adjustment, and multiplier.

3) **Segmentation**
   The iris part is detected by eliminating the upper and lower boundaries of eyelids, and eyelashes and central part of pupil boundary is done using the HT and Canny edge detection technique.

4) **Normalization**
   Segmented iris converted from the circular region (polar) into a rectangular region (cartesian) and normalization of iris image.

5) **Feature extraction**
   The normalized iris is converted into binary bit format using the Gabor filter technique and noise removal from iris image.

6) **Classification and matching**
   The difference between the 2 codes (iris input code and database eye image template code) is calculated using HD, and left and right shift operations are performed in order to get similarity between two images, and decision is made like Match/No match based on the matching score.

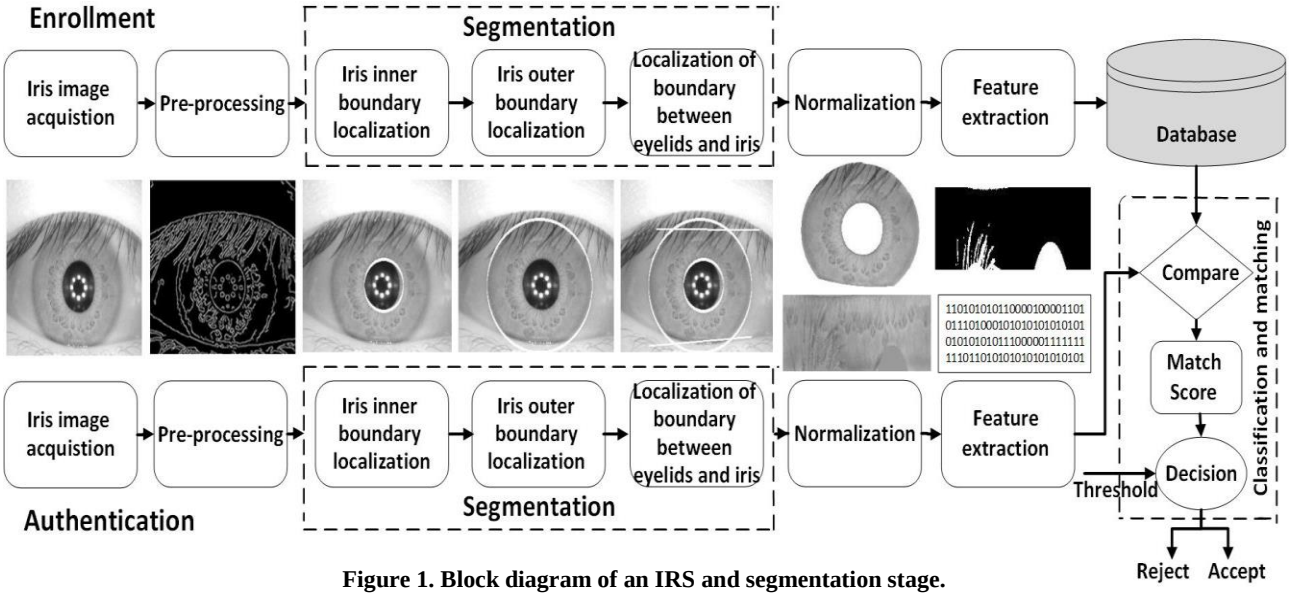

Figure 1. Block diagram of an IRS and segmentation stage.

2.1. Image acquisition

The first stage of IRS is image acquisition. Success of other recognition stages is reliant on the quality of the images taken from iris during image acquisition stage. This stage is very complicated because the size and color of iris in every person are different [19]. At this stage, we capture the iris images using different cameras or from the databases like UBIRIS, CASIA, MMUI, and BATH. The captured eye image must have a good quality along with a high resolution for Image processing, and if visible light is used during imaging, a slight contrast comes into existence between iris and pupil, which makes it hard to separate these two areas [20]. The UBIRIS, CASIA, MMUI, and BATH databases, which contain eye images, are used to test the proposed algorithm. The characteristics of the databases are given in table 1.

Table 1. Characteristics of the iris image databases.

Database	Number of images	Observations
BATH	16000	High homogeneous lighting environment. Containing essentially iris obstructions due to eyelids and eyelashes.
MMUI2	995	Noise factors avoided.
CASIA V3	22051	Image captured with two different devices. Containing images with close characteristics to the CASIA V1 version, with exception of the manual pupil filling.
UBIRIS	1877	Image captured under heterogeneous lighting environments. several reflections and obstructions can be observed.

2.2. Pre-processing

In the pre-processing stage, noise and eyelashes that may cover the iris region are detected and removed. The iris image has a low contrast and a non-uniform illumination caused by the position of the light source. All these factors can be compensated by the image enhancement algorithms. Initially, in order to do image enhancement and facilitate later processing, a primary processing is performed on iris images. In the pre-processing stage, Canny edge detection is used to enhance iris outer boundary and a multiplier function to enhance Canny iris points, and, also image contrast adjustment is performed to make its pixels brighter. Figure 2 shows a sample of an eye image, and the results of pre-processing stage performed.

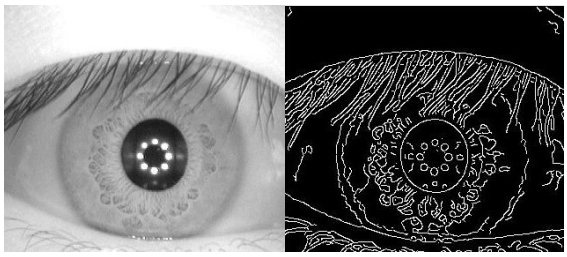

(a) **(b)**

Figure 2. (a) An eye image from CASIA database (b) the results of pre-processing performed.

2.3. Segmentation

In this Section, we discuss in detail the proposed iris segmentation method. It includes iris inner and outer boundaries localization, upper and lower eyelid and eyelash detection, which is useful for the next steps such as normalization, feature extraction and iris encoding, and matching process. A precise

iris image segmentation plays an important role in an IRS since success of the system in upcoming stages is directly dependent on the accuracy of this stage [21]. Figure 1 shows block of the segmentation stage and includes the 3 following stages:

1) **Localization of iris inner boundary.**
2) **Localization of iris outer boundary.**
3) **Localization of the boundary between eyelids and iris.**

HT is a standard computer vision algorithm that can be used to determine the parameters of simple geometric objects, such as lines and circles present in an image. The circular HT can be employed to deduce the radius and center coordinates of the pupil and iris regions [22]. These parameters are the center coordinates x_c and y_c, and the radius r, which are able to define any circle according to the following equation:

$$x_c^2 + y_c^2 - r^2 = 0 \qquad (1)$$

The parabolic HT is used to detect the eyelids. The mathematical relationship used to localize the upper and lower eyelids is gained with parabolic arcs, which is represented as:

$$(-(x - h_j)sin\theta_j + (y - k_j)cos\theta_j)^n = R \qquad (2)$$

where in

$$R = a_j\left((x - h_j)cos\theta_j + (y - k_j)sin\theta_j\right) \qquad (3)$$

where a_j controls the curvature, (h_j, k_j) is the peak coordinates of the parabola, and θ_j is the angle of rotation relative to the x –axis.

2.3.1. Iris inner boundary localization

Since pupil is a black circular region and darker compared with the iris, it is easy to detect the pupil inside an eye image. Firstly, pupil is detected using the thresholding operation. An appropriate threshold is selected to generate the binary image that contains pupil only. Since the inner boundary of an iris can be approximately modelled as circles, circular HT is used to localize the iris. Firstly, Canny edge detection is applied to binary image to generate the edge map. Figure 2 shows the results of performing Canny edge detection on an eye image as the pre-processing output. Figure 3 shows the iris inner boundary that has been achieved via this method for three eye images. As it is observable in figure 3, the method yields a boundary localized with a high accuracy.

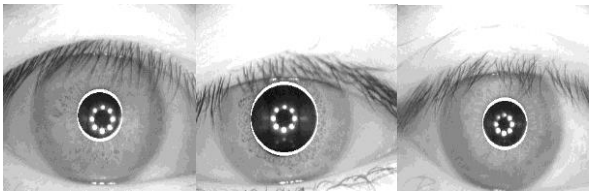

Figure 3. Iris inner boundary localized for three eye images.

2.3.2. Iris outer boundary localization

Too much blurring may dilate the boundaries of the edge or may make it difficult to detect the outer iris boundary, separating the eyeball and sclera. Thus a special smoothing filter such as the median filter is used on the original intensity image. This type of filtering eliminates sparse noise, while preserving image boundaries. After filtering, the contrast of image is enhanced to have sharp variation at image boundaries using histogram equalization. As a result, edge detection algorithms, which are able to detect outer iris edges, identify those points as edge. Therefore, in order to detect the iris outer boundary, these points have to be identified and eliminated. In this work, the available boundaries are initially enhanced, and then extra edge points are identified and eliminated. At the end, through circular HT, the outer iris boundary is obtained. In order to enhance iris the outer boundary edges, Canny edge detection is performed on eye image in the pre-processing stage. By performing such edge detection, a matrix is obtained with the same dimensions as of the image itself whose elements are high in areas where there is a definite boundary and the elements are low in areas where there is no perfectly definite boundary, such as iris outer boundary. Through multiplying of 2.76 in the matrix of pixel values of iris image and intensifying light in eye image, the edges are enhanced. Applying Canny edge detection and multiplying that to the constant value of 2.76 result in a better revelation of iris outer boundary edge points. It gains number 2.76 by trial and error, and by a little change, there is no accurate boundary recognition. Table 2 displays the accuracy rate of iris outer boundary localization for different values multiplying on three databases. As it is illustrated, with the multiplying value of 2.76, the most optimum accuracy rate in the iris outer boundary localization will be evident. Results of such application on three eye images are shown in figure 4. As it is observable in figure 4, the method yields a boundary localized with a high accuracy.

Table 2. Accuracy rate of iris outer boundary localization for different values multiplying on three databases.

Value	CASIA V1 (%)	CASIA V3 (%)	BATH (%)
1.50	87.12	86	87.10
2.00	93.37	92.12	93
2.76	**99**	**98.19**	**98.17**
3.00	94.12	94	92.38
3.50	91.73	90.67	89.34

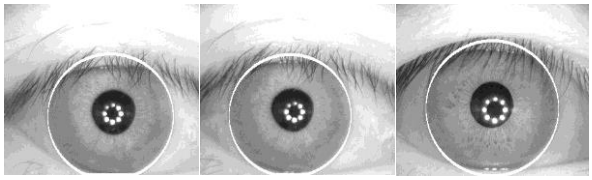

Figure 4. Iris outer boundary localized for three eye images.

The only issue of this method is sclera boundary not being circular, which is the result of angled or sideward imaging, and in these cases, some information is lost or clutter comes into existence. In this stage, after identifying the iris inner and outer boundaries, the results of these three stages are combined. Figure 5 shows the results obtained. As it could be seen in this figure, the iris inner and outer boundaries are correctly identified in the CASIA iris image-interval database.

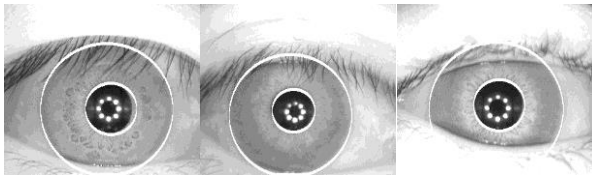

Figure 5. Iris inner and outer boundaries localized for three eye images.

2.3.3. Localization of boundary between eyelids and iris

Similar to the iris outer boundary localization, the proposed method selects two search regions to detect the upper and lower eyelids. The pupil center, iris inner, and outer boundaries are used as reference to select the two search regions. Canny edge detection is applied to the search regions to detect the eyelids. In order to reduce the false edges detection caused by eyelashes, Canny filter is tuned to the linear direction. After the edge detection step, the edge image is generated. The eyelids are detected using the parabolic HT method. The method calculates the total number of edge points in every linear row inside the search regions. The linear row with maximum number of edge points is selected as the eyelid boundary. If the maximum number of edge points is less than a predefined threshold, it is assumed that eyelid is not presented in the search regions. As it could be seen in figure 2, there are only pupillary edge points between the two eyelids, and since pupillary boundary has already been obtained, these points are eliminated. Figure 6 shows few boundaries localized through this method for some eye images. This method could result in a false outcome only for some images that have too many patterns in iris tissue when the edges of these patterns are detected by Canny edge detection. As it is observable in figure 6, the method localizes eyelids with a relatively high accuracy. Figure 6 exhibits samples of eye images in which eyelids are parabolic and linearly shaped. The boundaries of eyelids and iris are recognized properly but for those images in which eyelids are parabola shaped, this boundary is recognized with a slight discrepancy. The accuracy rate of the proposed method for the segmentation stage on different databases is presented in table 3. As the results presented in this table show, the method has an accuracy rate of between 97.6% and 99.63% for iris boundary localization.

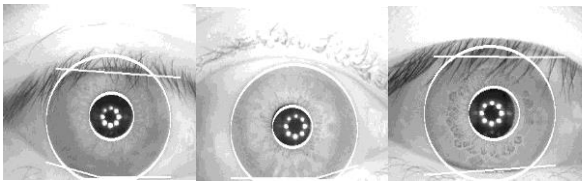

Figure 6. Boundaries between iris and eyelids localized for three eye images.

For the CASIA V1 and V3 databases, the segmentation technique managed to correctly segment the iris region from 747 out of 756 eye images, which corresponds to a success average rate of around 98.80%. The BATH images proved problematic and the segmentation process correctly identified iris and pupil boundaries for only 117 out of 120 eye images, which corresponds to a success average rate of around 97.98%. It is difficult to recognize the inner and outer iris boundaries for those images with small illumination intensity differences between the iris region, and the pupil region as shown in figure 7. For solving the problem, important parameters in imaging such as minimum and maximum radius of iris and pupil to search, threshold values for creating edge maps, camera hardware, imaging distance, and lighting conditions for each database, must be adjusted.

The eyelid detection system also proved quite successful, and managed to isolate the most occluding eyelid regions. One problem was that it would sometimes isolate too much of the iris region, which could make the recognition process less accurate, since there is less iris information. However, this is preferred over including too much

of the iris region, if there is a high chance it would also include undetected eyelash and eyelid regions. The eyelash detection system implemented for the CASIA database also proved to be successful in isolating most of the eyelashes occurring within the iris region, as shown in figure 6.

Table 3. Accuracy rate (AR) of iris boundary localization (BL) for three databases.

Iris Database	AR in pupil BL (%)	AR in sclera BL (%)	AR in eyelids BL (%)
CASIA Iris Image V1	98.13	99	99.31
CASIA Iris INTERVAL V3	99.63	98.19	98.58
University of BATH	98.18	98.17	97.60

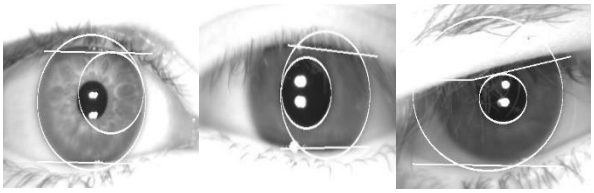

Figure 7. An example where segmentation fails for three eye images from BATH database

A slight problem was that areas where the eyelashes were light, such as at the tips that were not detected. However, these undetected areas were small when compared with the size of the iris region. Isolation of specular reflections from eye images in the MMUI database also proved to be successful. Numerous examples of their isolation are shown in figure 8.

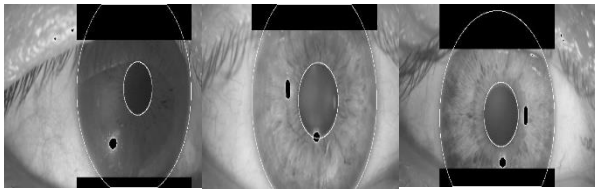

Figure 8. Automatic segmentation of various images from the MMUI database.

2.4. Normalization

For normalization of iris regions, a technique based on Daugman's rubber sheet model was employed. The center of the pupil was considered as the reference point, and radial vectors passed through the iris region. A number of data points are selected along each radial line, and this is defined as the radial resolution. The number of radial lines existing around the iris region is defined as the angular resolution. Since the pupil can be non-concentric to the iris, a remapping formula is required to rescale points depending on the angle around the circle. This is given by:

$$r' = \sqrt{\alpha\beta} \pm \sqrt{\alpha\beta^2 - \alpha - r_I^2} \quad (4)$$

where in

$$\alpha = o_x^2 + o_y^2 \quad (5)$$

$$\beta = \cos(\pi - \arctan(\frac{O_y}{O_x}) - \theta) \quad (6)$$

where displacement of the center of the pupil relative to the center of the iris is given by o_x, o_y, and r' is the distance between the edge of the pupil and edge of the iris at an angle, θ around the region, and r_I is the radius of the iris. The remapping formula first gives the radius of the iris region 'doughnut' as a function of the angle θ. Figure 9 shows transforming iris area from the polar to Cartesian coordinates. Therefore, iris area is obtained as a normalized strip with regard to iris boundaries and pupillary center. In this work, iris area is illustrated on a rectangular strip of 8*512 [23][26-27].

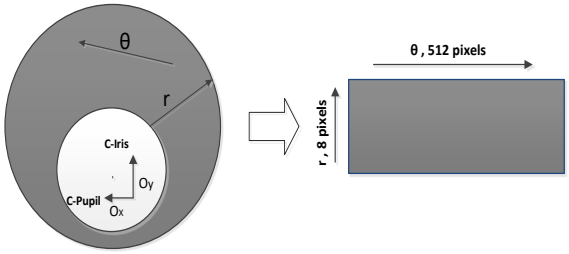

Figure 9. Transforming polar to Cartesian coordinates.

In order to transform iris area from polar to Cartesian coordinates, 128 pupils-centered perfect circles are chosen starting from iris-pupil boundary, and then the pixels are located on these circles that are next mapped into a rectangle (to change polar coordinates into the Cartesian). As a result, iris area, which looks like a circular strip, is converted into a rectangular strip. Choosing these 128 perfect circles normalizes iris in terms of size as well. Then illumination intensity was adjusted in segmented iris tissue, i.e. image contrast was applied to bring more clarity into iris tissue. Figure 10 shows a sample of normalized iris tissue [3].

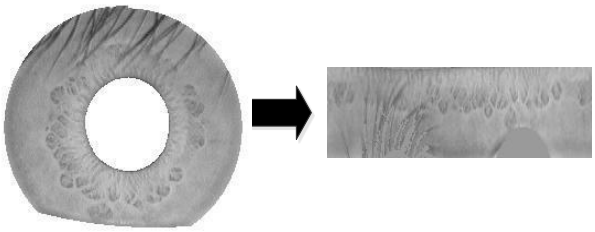

Figure 10. Transforming iris area into normalized rectangular strip.

2.5. Feature extraction and iris encoding

2D Gabor filters are used to extract iris features from the normalized iris image. A 2D Gabor filters is a Gaussian transfer function on a logarithmic scale [23]. It has strictly band pass filter to remove the caused background brightness and an ultimate feature vector is obtained. In this stage, the normalized iris is encoded in the form of binary bits (0, 1). In the coding system, the normalization image is converted to Gabor filter stage and Fourier for gaining iris image of feature extraction. Then iris image tissues become quantization, and finally, Quantization parameters are converted to binary. The dimensions of the feature vector extracted from iris area have to be as small as possible. Since vectors with large size, in respect of spatial, have high mass for saving, moreover, they have very high calculation mass in feature extraction and matching stage forcing system and decelerate. It regarding high dimensions of the image drawn, Gabor wavelet transform was performed in order to decrease the dimensions in the way that important information existing in tissue can be preserved in spite of downsizing image dimensions [14]. To do this, 2D Gabor wavelet transforms were conducted. Then the encoding obtained in this stage would be saved in dimensions of 80*240, and then enters the next stage of the system, namely the matching stage. Regarding that some sections of the area chosen for feature extraction may have occlusions caused by eyelids and eyelashes and since it is possible that because of error in segmentation stage some parts of sclera are subjected to be detected as iris area, it is required that a measure be taken to remove these points from the feature extraction stage. To resolve the latter issue that is caused by error when detecting iris outer boundary, 20% of the lower section of the image is eliminated, and to resolve the first issue, points of the image that are placed in this section are eliminated from encoding. To do this, a binary encoding that detects occlusion points is produced. This encoding is implied in the matching stage, and these points are eliminated in that stage [25].

2.6. Classification and matching

For matching, HD was chosen as a metric for recognition, since bit-wise comparisons were necessary. The HD algorithm includes calculation of differences for the 2 codes and the noise masking in a way that only significant bits are used in calculating the HD between two iris template codes. Now when taking HD, only those bits in the iris pattern that correspond to '0' bits in noise masks of both iris patterns will be used in the calculation. HD will be calculated using only the bits generated from the true iris region, and this modified HD formula is given as

$$HD = \frac{1}{N - \sum_{K=1}^{N} X_{n_k}(OR)\, Y_{n_k}} * M \quad (7)$$

where in

$$M = \sum_{j=1}^{N} X_j(XOR)\, Y_j(AND) X'_{n_j}(AND) Y'_{n_j} \quad (8)$$

where, X_j and Y_j are the two bit-wise template codes to compare, X'_{n_j} and Y'_{n_j} are the corresponding noise masks for X_j and Y_j, while N is the number of bits represented by each template code. If the value for feature vector in point (X, Y) is equal to the value for other feature vector in that point, digit 1 is allotted to that point, and if they are not equal, digit 0 is done. Then the values allotted to the pixels are summed up and similarity criterion of the two images is attained. One important factor in the matching stage is rotation of the incoming image. With respect to the position of the individual's head at the time of imaging, it may be that the individual's head and eye direction are in different positions each time, and that causes the imbalance of the images taken from eyes. To resolve rotation issue, feature vector is rotated and relocated, and encoding is done for several images obtained through rotating original image instead of just one image, and matching is done for all of them, and then the lowest value, among other calculated values, is considered as the matching criterion.

Because iris circular strip in the normalization stage is transformed to the horizontal strip, movement is on the horizontal direction on encoding equivalent with iris area rotation, and rotation direction is related to movement direction on the encoding. Since the 360 degrees of iris section are registered as a 512 strip, movement of 2 bits on horizontally- registered strip equals rotation of 90 degrees in iris section. Figure 11 displays iris encoding transference to the left and right sides, and finding the best matching of HD as well.

3. Experimental results

In various databases, a perfect recognition is not possible due to the overlapping distributions. Hence, at first, it must mark value threshold. As it is clear in table 4, for value threshold 0.4, false accept rate (FAR) and false reject rate (FRR) 0.12%, 1.08% are obtained, respectively. This value among the values in table 4 in respect of

FAR, FRR is the best value threshold. Therefore, if two irises are identical, their HD value must be below 0.4 and if two irises are distinctive, their HD value must approximate or exceed 0.4. Efficiency of a biometric system is usually evaluated by taking into account FAR and FRR.

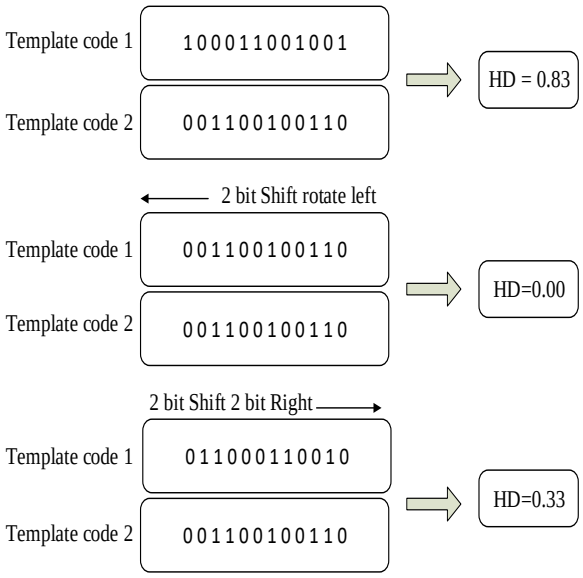

Figure 11. Transference of iris encoding to left and right side and finding best matching of HD.

Table 4. FAR and FRR for the CASIA database with different value threshold using the optimum parameters.

Threshold	FAR (%)	FRR (%)
0.20	0.000	99.047
0.25	0.000	82.787
0.30	0.000	37.880
0.35	0.000	5.181
0.40	**0.12**	**1.08**
0.45	7.599	0.000
0.50	99.499	0.000

Evaluated as more efficient, FAR means how many people the system mistakenly accepts when they introduce someone instead of others. FRR means how many people with entrance allowance are not recognized by the system and are announced as errors.

The FAR rate is calculated in off-class distribution of P_{diff} regarding the normalized area between zero and K value threshold. The FRR rate equals the normalized area between value threshold and a point in in-class distribution of P_{same}.

$$FAR = \frac{\int_0^K P_{diff}\ (x)dx}{\int_0^1 P_{diff}\ (x)dx} \tag{9}$$

$$FRR = \frac{\int_k^1 P_{same}\,(x)dx}{\int_0^1 P_{same}\,(x)dx} \tag{10}$$

In table 5, the results of the proposed method for two different databases have gained base on Equations (9) and (10). According to the table, accuracy rate of the proposed method on the CASIA database is 98.8% that is a rather proper accuracy. The reason the low accuracy attained for the BATH database is the very low illumination intensity differences in iris and pupil boundary in their images.

Table 5. FRR and FAR for two different databases with threshold of 0.4.

Iris Database	FAR (%)	FRR (%)	System Accuracy (%)
CASIA Iris Interval	0.12	1.08	98.80
University of BATH	2.02	0	98.80

The segmentation error rate, E_i, per image is given by the fraction of disagreeing pixels between the ground-truth image and the output image produced by the proposed method:

$$E_i = \frac{1}{m * n}\sum_{x=1}^{m}\sum_{y=1}^{n} C(x,y) \otimes O(x,y) \tag{11}$$

where, E_i is the segmentation error rate per image i, $C(x,y)$ and $O(x,y)$ are two pixels from the ground-truth and the output images, the operator $\otimes$ refers to the Boolean XOR, and m and n are the height and width of the image, respectively. The overall segmentation error rate, E, is then calculated as the average segmentation error rates over all images:

$$E = \frac{1}{N}\sum_{i=1}^{N} E_i \tag{12}$$

where, N is the number of tested images, and E_i is the segmentation error rate per image i, which is calculated by Equation (11). Mainly, E ranges between 0 and 1 interval, value 0 represents the optimal error rate, and the worst error rate occurs when E equals 1. In table 6, the performance results of several popular algorithms of IR with the proposed method on the MMUI, UBIRIS, and CASIA database images are presented.

As seen in the table, the accuracy rate of the proposed method is higher than the Ma algorithm and it is very close to the accuracy rate of the Yahya algorithm [20]. It should be mentioned that the reason for very high accuracy of the Daugman's method is their strict standards regarded at the time of imaging. Parabolic HT is used for eyelids localization; therefore, the speed of the proposed

algorithm is more than the speed of others such as parabolic HT in the stage of iris localization [24].
The proposed approach is better than all the recent methods used with the MMUI and UBIRIS databases, and compared to the CASIA database, only the Daugman's method is a bit better, since the conditions that Daugman's considers for imaging is a very restrictive and specific condition. However, recent IRSs have focused on images acquired in unconstrained environments. These imaging environments allow the capture of iris images at a distance, in motion, and under visible wavelength illumination, which lead to more noise factors such as off-focus, gaze deviation, and obstruction by eyelids, eyeglasses, hair, lighting, and specular reflections.
As it is evident in table 5, the proposed algorithm on 386 different images from equal databases was conducted and the researchers' algorithm results were elicited from referenced tables [2, 28-30]. The number of images and databases are equal throughout the present contrastive comparison but the images are not. The major purpose is to determine the state and the rate of satisfaction of the proposed method among the recognized comparative algorithms. As it is evident, the proposed method, has a significant satisfiable state in this algorithm.

Table 6. Efficiency comparison on MMUI, UBIRIS and CASIA database images for popular algorithms (Overall Accuracy (OA), Segmentation Error Rate (E), UBIRIS).

Algorithm	OA (%) CASIA	OA (%) UBIRIS	OA (%) MMUI	E (%) UBIRIS	E (%) CASIA
Umer [11]	97.92	97.51	97.78	1.10	1
Ma [10]	87.27	95.79	95.11	1.63	1.75
Jan [12]	96.75	97.65	96.30	2.50	3.00
Tan [7]	98.20	93.6	----	1.90	1.09
Radman[2]	98.40	----	92.67	1.60	----
Daugman's[3]	99.90	97.29	90.59	1.52	0.77
Proposed method	**98.80**	**99.12**	**98.34**	**1.35**	**0.83**

Provided that N number of images in the system are registered, that is N number of images be used for education, the accuracy of identity recognition will differ. Table 7 presents the accuracy of the system per number of images registered for each person. As it is evident, with 10 images for each person, the accuracy of identity recognition increases.
The proposed method of identity recognition was done on 386 iris images from databases BATH and CASIA.

Table 7. Comparing identity distinction precise of proposed method with Daugman's method based on register teaching picture number (N=1, 3, 5, 7, 10).

Picture Number (N)	Daugman's method (%)	proposed method (%)
1	96	96.3
3	96	96.8
5	96	97
7	96	97.6
10	96	98.80

Due to probability equality for each extracted bit for iris being 0 or 1, if 2 codes are produced for 2 virtual irises, HD value difference will probably equal 0.4. Therefore, if 2 irises are identical, the HD value should be lower than 0.4 and if they are distinctive, their HD value will approximate or even exceed 0.4. The bigger the HD value than 0.4, the more safely a decision could be made. Consequently, the system success rate equals 98.80% on the CASIA database and is comparable with other methods of IR available utilizing iris images. The failure of 1.2% in iris segmentation stage is due to those images in the database that bear an extremely low color contrast intensity at the border of iris and pupil. The system success rate equaled 97.98% on the BATH database. The reason for this lower accuracy for the BATH database is that the difference of light intensity is extremely low at the border of iris and pupil. FRR and FAR with standard deviation of 0.4, system general accuracy, and the curve relating to relative operating characteristic (ROC) of the proposed method are exhibited in figure 12. Based on this figure, the best threshold value equals 0.4, which results in the error rate of E=0.83%, that is identity acceptance will be done with 98.80% of accuracy. Since each iris has 10 images in database, identity recognition could be done in a way that input image accords at least with N images. ROC curve relating to N = 3, 5, 7, 10 are presented in figure 13. Also, in figure 14, the results of the proposed method on the CASIA databases are shown.

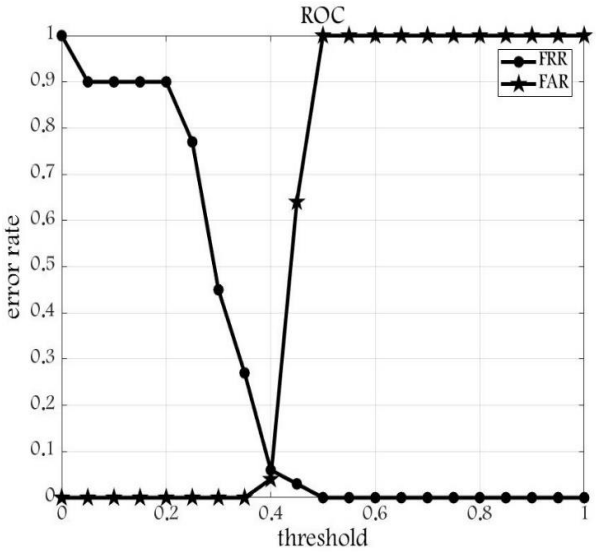

Figure 12. Curve ROC relateds to proposed method.

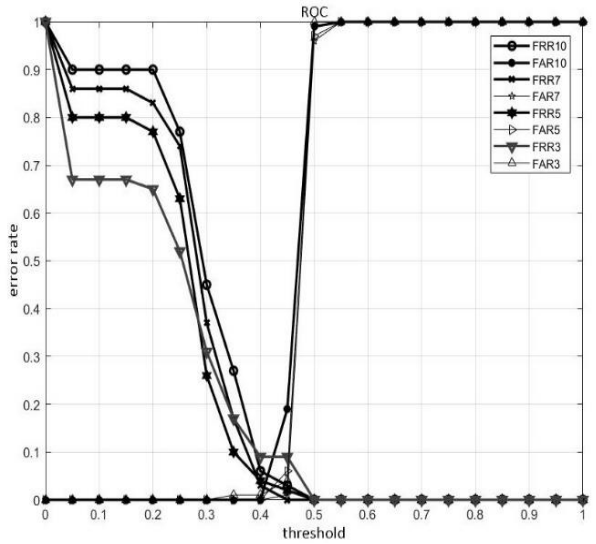

Figure 13. Curve ROC relateds to proposed method with regard to adoptions numbers (N= 3, 5, 7, 10).

4. Conclusion

The accuracy of IRS is dependent on the performance of the iris segmentation method. This paper presented an effective and robust method of iris segmentation for IR in unconstrained environments by performing HT. In this method, the pupil's boundary and the iris boundary were localized with high accuracy. Despite variations of illumination intensity in iris outer boundary compared with other sections of the eye, a very high accuracy rate was achieved for the proposed method. Also, after recognizing the boundaries, the iris section is separated from the human eye and entered the normalization and feature extraction and iris encoding. The wrong determination of iris images will affect the normalization results. This is due to a non-uniform distance between the inner and outer iris boundaries. The results of examining the method on the UBIRIS, CASIA, MMUI, and BATH database images indicated the efficiency and high accuracy of the proposed method, which is comparable with other existing methods for identity recognition using iris images. The recognition time will not change when the iris determination is correctly or wrongly evaluated because it is an independent variable in the iris size. Researchers interested in following the lines drawn in this paper, may utilize oval-shaped model in IRSs, utilize parabolic model in eyelid recognition, or project IRS on GPUs with CUDA in order to accelerate the execution.

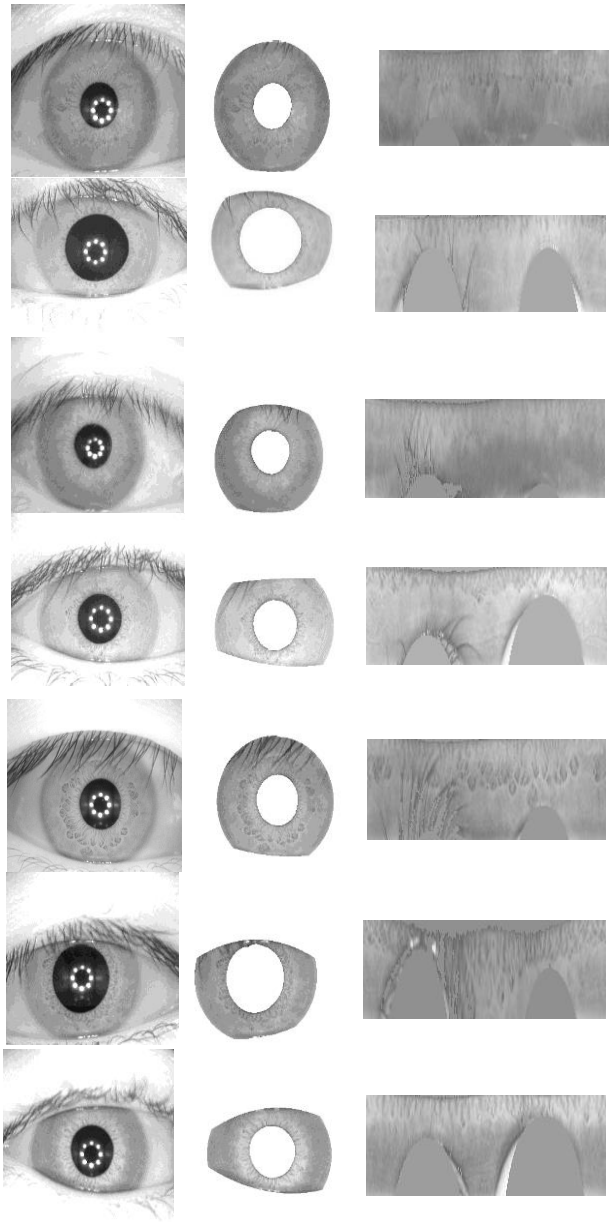

(a) (b) (c)

Figure 14. Results of the proposed method on CASIA databases: (a) Original image (b) Segmented image (c) Output of the normalization stage.

References

[1] Jain, A. K., Ross, A. & Pankanti, S. (2006). A Tool for Information Security. IEEE Transactions on Information Forensics and Security, vol. 1, pp. 125-143.

[2] Radman, A., Zainal, N. & Suandi, S. (2017). Automated segmentation of iris images acquired in an unconstrained environment using HOG-SVM and GrowCut. Journal of Digital Signal Processing, vol. 64, pp. 60-70.

[3] Daugman, J. G. (2007). New methods in IR. IEEE Transactions on Systems, Man and Cybernetics, vol. 37, pp. 1167-1175.

[4] Wildes, R. (1997). IR: an emerging biometric technology. Proceedings of the IEEE, vol. 85, pp. 1348-1363.

[5] Kong, W. & Zhang, D. (2001). Accurate iris segmentation based on novel reection and eyelash detection model. In International Symposium on Intelligent Multimedia, Video and Speech Processing, pp. 263-266.

[6] Hu, Y., Sirlantzis, K. & Howells, G. (2015). Improving colour iris segmentation using a model selection technique. Journal of Pattern Recognition, vol. 57, pp. 24-32.

[7] Tan, C. W. & Kumar, A. (2012). Efficient iris segmentation using grow-cut algorithm for remotely acquired iris images. In 5th IEEE International Conference on Biometrics: Theory. Applications and Systems (BTAS), pp. 99-104.

[8] Dorairaj, V., Schmid, A. & Fahmy, G. (2005). Performance evaluation of iris based recognition system implementing PCA and ICA encoding techniques. In Proceedings of SPIE 5779, pp. 51-58.

[9] Fancourt, C., Bogoni, L., Hanna, K., Guo, Y., Wildes, R., Takahashi, N. & Jain, U. (2005). IR at a distance. In Proceedings of the International Conference on Audio and Video-Based Biometric Person Authentication, pp. 1-13.

[10] Ma, L., Tan, T., Wang, Y. & Zhang, M. (2004). Effcent iris recognition by characterizing key local variations. IEEE Transactions on Image Processing vol. 13, pp. 739-750.

[11] Umer, S., Dhara, B. C. & Chanda, B. (2016). Texture code matrix-based multi-instance IR. Springer Pattern Ana, vol. 19, pp. 283-295.

[12] Jan, F., Usman, I. & Agha, S. (2013). Reliable iris localization using HT. histogram-bisection and eccentricity, Springer Signal Process, vol. 93, pp. 230-241.

[13] Rathgeb, C., Uhl, A. & Wild, P. (2014). Effects of severe image compression on iris segmentation performance. Proceedings of the IEEE/IAPR International Joint Conference on Biometrics (IJCB14), pp. 22-28.

[14] Chen, Y., Adjouadi, M., Barreto, A., Rishe, N. & Andrian, J. (2009). A computational efficient iris extraction approach in unconstrained environments. in BTAS09 Proceedings of the IEEE International Conference on Biometrics, Applications and Systems, pp. 17-23.

[15] UBIRIS dataset obtained from Department of Computer Science, University of Beira Interior, Portugal. Available from: http://iris.di.ubi.pt/.

[16] CASIA-IrisV3 Interval database. Available from: http://www.cbsr.ia.ac.cn/english/IrisDatabase.asp.

[17] MMU1 and MMU2 iris databases. Available from: http://pesona.mmu.edu.my/∼ccteo/.

[18] Bath iris image database. Available from: http://www.smartsensors.co.uk/products/iris-database/.

[19] Subha, R. & Pushpa Rani, M. (2017). Wavefront Coding for Iris Recognition, International Journal of Scientific Research in Computer Science, Engineering and Information Technology, vol. 2, pp. 89-92.

[20] Yahya, A. E. & Nordin, M. J. (2008), A new technique for iris localization in IR system. Information Technology Journal, vol. 7, pp. 924-928.

[21] Masek, L. (2003), Recognition of human iris patterns for biometric identification. B. S. Dissertation, The School of Computer Science and Software Engineering, The University of Western Australia, Crawley WA, Perth, Australia.

[22] Memar Zadeh, S. & Harimi, A. (2017). Iris localization by means of adaptive thresholding and circular Hough transform. Journal of Artificial Intelligence & Data Mining (JAIDM), vol. 5, pp. 21-28.

[23] Turner, M. R. (2013). Texture discrimination by Gabor functions, Cybernetics, vol. 55, pp. 71-82.

[24] Shah, S. & Ross, A. (2009). Iris segmentation using geodesic active contours. IEEE Transactions on Information Forensics and Security, vol. 4, pp. 824-836.

[25] Yang, H., Konstantinos, S. & Gareth, H. (2017). A novel iris weight map method for less constrained IR based on bit stability and discriminability. Image and Vision Computing, Elsevier, vol. 58, pp. 168-180.

[26] Trokielewicz, M., Czajka, A. & Maciejewicz, P. (2017). Implications of ocular pathologies for IR reliability. Image and Vision Computing, Elsevier, vol. 58, pp. 158-167.

[27] Bergmller, T., Christopoulos, E., Fehrenbach, K., Schnll, M. & Uhl, A. (2017). Recompression effiects in IR. Image and Vision Computing, Elsevier, vol. 58, pp. 142-157.

[28] Ouabida, E., Essadique, A. & Bouzid, A. (2017). Vander lugt correlator based active contours for iris segmentation and tracking, Expert Systems with Applications, vol. 71, pp. 383-395.

[29] Mahlouji, M. & Noruzi, A. (2012). Human Iris Segmentation for Iris Recognition in Unconstrained

Environments. IJCSI International Journal of Computer Science Issues, vol. 9, pp.149-155.

[30] Umer, S., Chandra Dhara, B. & Chanda, B. (2017). Novel cancelable iris recognition system based on feature learning techniques, Information Sciences, Elsevier, vol. 406, pp. 102-118.

[31] Kaushik, R., Prabir, B. & Ching, Y. (2011). Iris segmentation using variation level set method, Optics and Lasers in Engineering, Elsevier, vol. 49, pp. 578-588.

[32] Jan, F. (2016). Segmentation and localization schemes for non-ideal iris biometric systems, Signal Processing, Elsevier, vol. 133, pp. 192-212.

نشریه هوش مصنوعی و داده کاوی

سیستم شناسایی عنبیه چشم انسان در محیط‌های بدون محدودیت

علی نوروزی[1]، محمود محلوجی[2,*] و علی شهیدی نژاد[1]

[1] دانشکده فنی و مهندسی، گروه کامپیوتر، واحد قم، دانشگاه آزاد اسلامی، قم، ایران.

[2] دانشکده برق و کامپیوتر، گروه برق، واحد کاشان، دانشگاه آزاد اسلامی، کاشان، ایران.

ارسال ۲۰۱۸/۰۹/۰۶؛ بازنگری ۲۰۱۹/۰۲/۲۲؛ پذیرش ۲۰۱۹/۰۵/۰۸

چکیده:

یک سیستم بیومتریک، شناسایی خودکار یک فرد را بر اساس ویژگی منحصر به فرد، متعلق به فرد فراهم می‌کند و با گذشت زمان تغییر نمی‌کند. شناسایی عنبیه قطعی‌ترین و صریح‌ترین سیستم شناسایی بیومتریک می‌باشد. سیستم شناسایی عنبیه شامل مکانیزم قطعه‌بندی خودکار است که بر مبنای تبدیل هاف کار می‌کند. تشخیص عنبیه اساسا به شش مرحله تقسیم می‌شود، تصویربرداری، پیش‌پردازش، قطعه‌بندی، نرمال‌سازی، استخراج ویژگی و انطباق. در این روش، ابتدا عکس از عنبیه گرفته می‌شود، سپس تشخیص لبه انجام می‌شود، بعد از آن یک تنظیم کنتراست در مرحله پیش‌پردازش مورد استفاده قرار می‌گیرد. سپس از تبدیل هاف دایره‌ای برای مکان‌یابی بخش دایره‌ای شکل مرزهای داخلی و خارجی عنبیه استفاده شده است. همچنین با به کارگیری تبدیل هاف سهمی گونه، مکان‌یابی مرز پلک‌های بالا و پایین چشم که با بخش عنبیه تداخل دارد انجام شده است. روش پیشنهادی، در مقایسه با سیستم های شناسایی عنبیه موجود، نه تنها دارای دقت درستی نسبتا بالاتری بوده بلکه از لحاظ زمان پردازش با آنها رقابت می کند. نتایج پیاده‌سازی روش فوق روی تصاویر موجود در پایگاه داده‌های UBIRIS، BATH، CASIA و MMUI نشان می‌دهد که روش پیشنهادی دارای دقت درستی به ترتیب ۹۹،۱۲٪، ۹۷،۹۸٪، ۹۸،۸۰٪ و ۹۸،۳۴٪ می‌باشد.

کلمات کلیدی: تبدیل هاف، شناسایی بیومتریک، قطعه بندی، نرمال سازی، انطباق.